Contents

Chapter 1

Introduction

1.1 Background

One of the most well known problems in quantum mechanics, and therefore an area that receives a lot of attention, is the circumvention of the 'curse of dimensionality'(1,2). This has been summarised sufficiently in a quote by Dirac where he states that the equations necessary to understand chemistry are largely known and that the scientific community merely lacks the capacity to solve them. This is most evident in the fact that every additional degree of freedom in the quantum Hamiltonian generates an exponential increase in computational cost, leading to the simulation of systems of interest to be incredibly time consuming in the best case, and impossible in the worst. The way that quantum mechanics has to advance is therefore not by discovering new still unknown laws of chemistry, but inventing new numerical methods that provide more accessible solutions to the Schrodinger equation. This innovation is necessary as purely classical approaches such as those by Karpus *et al*(3), were computationally feasible but ignored quantum ideas such as zero point energy and tunneling(4-6), whereas entirely quantum approaches require an extreme computational cost.

Such innovations began with semiclassical methods, aiming to combine the relative computational simplicity of classical approaches while maintaining some detail and influence of quantum concepts(7). One of the first relevant and notable semiclassical approaches was published in the 1970s by Miller *et al* called the Initial Value Representation (IVR)(8-10). IVR had an computational advantage over the purely quantum systems due to replace the fully quantum scattering matrix with an approximation matrix containing classical terms only. However, this

semiclassical venture wasn't sufficient as the method still required the extensive search for well behaved classical trajectories(11,12), which resulted in IVR being too expensive for research beyond the case study system of the H_2+He system.

Also in the 1970s, Heller *et al* introduced the idea of frozen Gaussian wave packets(13-15). Much of a quantum system can be written in the form of a superposition of frozen w wave packets, including both the initial and final wavefunction, and these wave packets are incredibly versatile even being capable of replacing the trajectories. These new trajectories are capable of maintaining the average position and momentum of the coinciding classical trajectory throughout the entirety of the propagation, resulting in a greatly reduced computational cost. This approach proved useful as it was applied to scattering problems and generated accurate results(16). As is common in science, this idea of frozen Gaussian wave packets was expended upon by multiple different authors with the addition of helpful prefactors(17,18) and new derivations were provided which aided in removing several criticisms(11). These improvements continued and this approach has proven successful and useful enough to still be used in the methods of today(1,21,22), or at least inspire current innovations.

An incredibly useful tool of fully quantum approaches is that of coherent states (CS)(23,24). The idea of the coherent state is almost as old as quantum mechanics itself, with Schrodinger presenting them as the wave packets of minimum uncertainty of the quantum harmonic oscillator(25). Presently, CS are known to be the states of minimum uncertainty with regards to Heisenberg's uncertainty principle for an increased number of systems(24). CS can also be understood from an operator viewpoint, as CS are the result of applying a displacement operator on a vacuum state and they also serve as the eigenvalues of the creation and annihilation operators. Given its prevalence throughout quantum mechanics, CS provide an almost classical level of ease of understanding and computation while maintaining the entirely quantum aspect of a state that is needed to capture all the relevant information of a quantum system, akin to how Ehrenfest's theorem(26) can connect the classical equations of motion with the expected position and momentum of the quantum world.

A singular coherent state is capable of representing simple harmonic oscillator systems but modern quantum systems of interest are too complicated for a single CS to suffice. Instead, a basis set can be formed from multiple CS which when combined with appropriate trajectories can allow for an improvement in computational time(27,28) and leading to an aptly named trajectory

guided basis set. A rigid grid style basis is a perfect example of the curse of dimensionality where for a number of points, l, in a grid that has M dimensions requires a basis set of size l^m. A trajectory guided basis set is capable of using considerably fewer basis functions as it is capable of essentially highlighting the key areas of phase space needed to represent the system. It also allows so-called 'on the fly' Ab Initio Molecular Dynamics (AIMD)(29-39) in which the potential energy surface (PES) can be recalculated while the basis set is propagating.

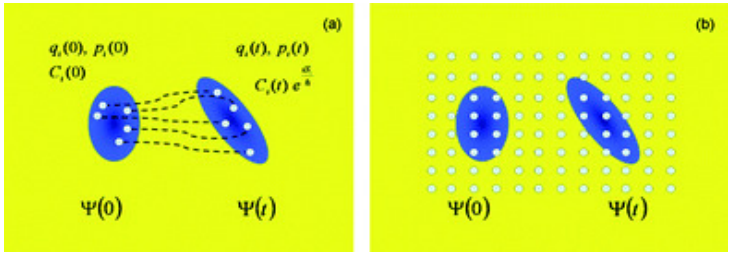

Figure 1.1: Image showing the different representations of the same phase space provided by a rigid grid (right) compared to a basis of coherent states guided by trajectories (left). Copied from [2].

In 2000, Shalashilin *et al* published the method of Couple Coherent states (CCS), which employed CS in order to model a Morse potential(40). When compared to the benchmark, CCS saved computational time by removing the need to invert costly unstable overlap matrices, as they often result in non invertible singularities. CCS is also a fully quantum approach which with the use of phase space co-ordinates is capable of producing exact quantum amplitudes(41), given a large basis set the result will converge to the entirely quantum result. Later, CCS was used for much larger systems(42-45) than the original presented and was capable of producing accurate spectroscopy results(46), proving its usefulness enough to be used in recent research(47,48).

1.2 MCE

Shalashilin *et al* later published the Multiconfigurational Ehrenfest method (MCE)(28) which expanded CCS to allow simulation of more than 1 PES. MCE currently has 2 versions, MCE version 1 (MCEv1) and MCE version 2 (MCEv2)(49), both of which were tested against the usual benchmark for spin boson two level systems, Multiconfigurational Time Dependent Hartree (MCTDH)(50-58). This approach uses the variational principle across the entire wavefunction, which itself is construed as a summation of multiple single particle functions. This method produces results with a high level of numerical accuracy, making it a prime choice as a comparative

benchmark. However, MCTDH still suffers from the curse of exponential scaling, meaning MCE could prove could be computationally cheaper if it can provide the accurate results produced by MCTDH, MCE might be capable of presenting results to a MCTDH standard for systems with 100s of degrees of freedom.

A key idea in the convergence of MCEv2, and the inspiration for my research, is cloning. Along with numerous sampling methods (trains and pancakes), cloning was initially required in order to converge MCEv2 and generate results that agree with the benchmark. Cloning involves creating an additional basis function (or basis set in extreme cases) in order to better represent certain areas of phase space. MCEv2 with the addition of cloning forms the basis of Ab Intio Multiple cloning (AIMC)(59-61), which has been used in multiple circumstances.

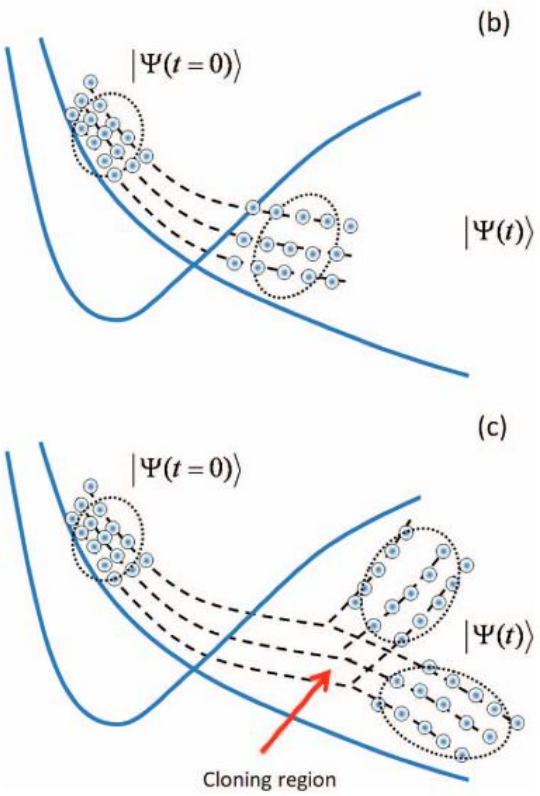

Figure 1.2: The cloning procedure shown creating 2 sets of basis functions and placing one set on the above PES and another on the lower PES in an attempt to assist issues with Ehrenfest trajectory propagation. Copied from [60].

AIMC is most useful when investigating ultra-fast photochemistry(59), producing accurate simulations of real molecules undergoing non-adiabatic transitions. AIMC is well-suited as 'ultra-fast photochemistry on the subpicosecond timescale is an essentially quantum process'(2). Important photochemistry occurs across nature, including the lessening the harmful effects of UV

rays interacting with DNA(62-64) and in the mechanisms of photon pumps(65) such as the ones necessary for vision, including bacteriorhodopsin(66-72).

Beyond the population of states results initially presented by MCE, the method can also be employed to produce vital information, including detailed spectra. In 2015, AIMC was used to study the molecule pyrrole, producing accurate total kinetic energy release (TKER) spectrum(73) of pyrrole photodissociation(74,75), with corresponding velocity maps. This paper argues an excellent use case of MCE as the method is capable of producing a detailed simulation under the same conditions as specific experiments in order to corroborate findings, which in this case, supported the findings and the mechanism proposed for the dissociation of the N-H bond.

The simulations are detailed to the extent of being capable to simulate the difference between pyrrole and deuterated pyrrole, taking into account the isotropic effect and pre-excitation of the N-H/N-D bond(76) causing the oscillation strength difference. These simulations confirmed the idea put forward by the experimental research and previous calculations(77-78) that only pre-excitation of the N-D bond is capable of generating the high-energy levels found.

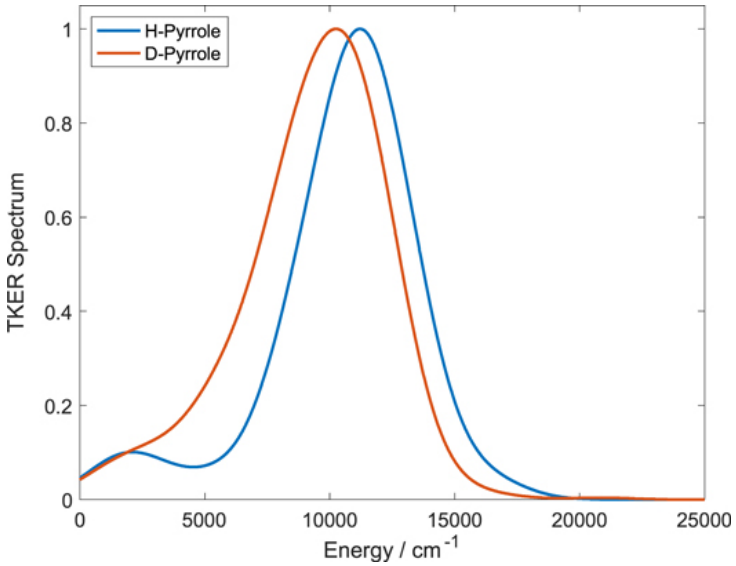

Figure 1.3: TKER spectrum produced by AIMC showing the photodissociation of pyrrole (blue) and deuterated pyrrole (red) Copied from [78].

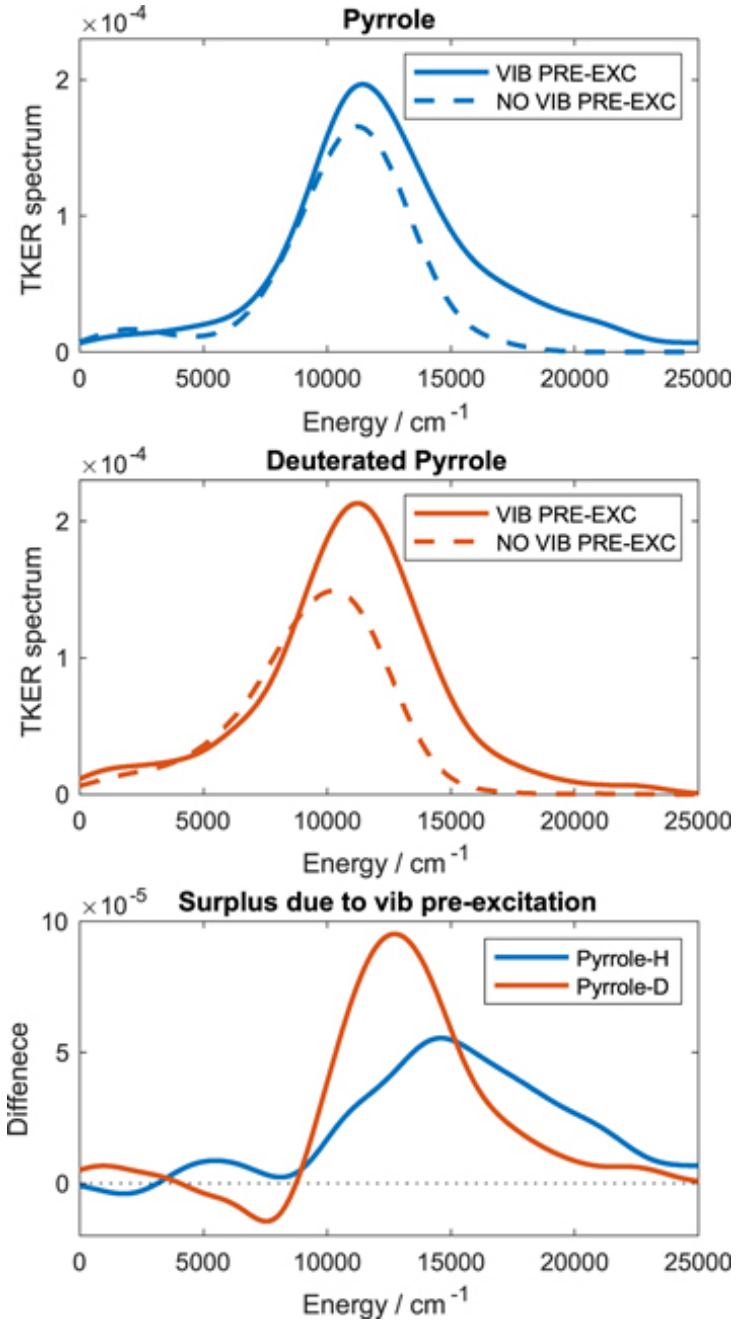

Figure 1.4: The TKER spectrumc comparing vibrational pre-exication (full line) with no pre-excitation (dotted line) for the dissociation of both pyrrole (above) and deuterated pyrrole (below). Calculated by AIMC-MCE. Copied from [78].

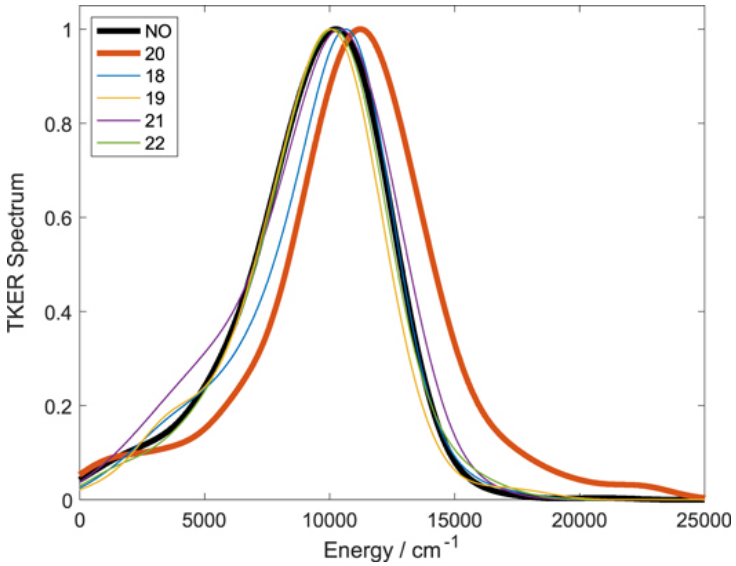

Figure 1.5: The effect of pre-exicatoin of vibrational moddes on the TKER spectra of the photodissociation deuterated pyrrole. Copied from [78].

The final conclusion to take from this paper is that it was able to provide information about deuterated pyrrole that hadn't yet been discerned from experiments. Makhov *et al* noted in the spectra for deuterated pyrrole that 'the integral increase of dissociation yield is surprisingly higher for D-pyrrole'(76), which is an example of the pinnacle of MCE. Not only is the method capable of corroborating and verifying information from experiments but also can provide potential new avenues for research with information that can be calculated efficiently due to the quick nature of MCE.

Matching the frequency and strength of the oscillations of spin boson systems in a lengthy time frame has proven to be an issue for many methods and approaches, including MCEv1. Despite being able to produce near identical results initially, the high number of degrees of freedom needed to simulate the required bath modes are difficult to compute. A potential solution to rectify these issues is the introduction of cloning procedure as it was a vital ingredient in the convergence of MCEv2 for a large number of cases. However, due to the differing ansatz used for both MCEv1 and MCEv2, the form of cloning that could possibly be implemented is an adaptation of previous methods, with the hope of eventually providing similar boons.

Chapter 2

Theory

This chapter presents a simplified derivation where all equations are using atomic units where $\bar{h} = 1$, tidying up the equations without losing any accuracy. All equations relating to MCE have also been restricted to only 2 PES, as the expansion to general case is unnecessary as it does not feature heavily in current publications. The last notable notation is that all of the quantum Hamiltonian are in their ordered form. where the Hamiltonian is rewritten such that the annihilation operators (with their respective powers) proceed the powers of the creation operators. MCE makes use of phase space coordinates, with p and q denoting momentum and position respectively with $\hat{P}$ and $\hat{Q}$ denoting their respective quantum operators.

2.1 Multiconfigurational Ehrenfest method

MCE utilises the Ehrenfest assumption, separating the full system Hamiltonian into two separate Hamiltonians. The first represents the quantum system while the second represents the classical bath environment containing the information concerning the interaction between them within a final potential term.

$$\hat{H}(\hat{P}, \hat{Q}, p, q) = \hat{H}^{ssytm}_{qntm}(\hat{P}, \hat{Q}) + \hat{V}_{int}(\hat{P}, \hat{Q}, p, q) + \hat{H}^{bath}_{cl}(p, q) \tag{2.1}$$

This assumption simplifies several equations and allows the trajectories to be guided by Hamilton's equations, such that $p(t)$ and $q(t)$ are given by,

$$\dot{q} = \frac{\partial H_{Ehr}}{\partial p}, \dot{p} = \frac{\partial H_{Ehr}}{\partial q} \tag{2.2}$$

. The Ehrenfest Hamilton H_{Ehr} is a weighted superposition of time independent basis wave functions. This is calculated by averaging the total Hamiltonian over the wave function of the entire system as follows,

$$H_{Ehr} = \langle \Psi^{sstm}(t) | \hat{H}(\hat{P}, \hat{Q}, p, q) | \Psi^{sstm}(t) \rangle \tag{2.3}$$

$$\Psi^{sstm}(t) = a_1(t) | \phi_1^{sstm} \rangle + a_2(t) | \phi_2^{sstm} \rangle + \cdots \tag{2.4}$$

These amplitudes, $a(t)$, are time dependent and therefore the change in wavefunction can modeled entirely through the evolution of these quantum amplitudes. The derivatives of these amplitudes are found by the use of the following common coupled equations,

$$\frac{da_i}{dt} = -\frac{i}{h} \sum \langle \phi_i | \hat{H}(\hat{P}, \hat{Q}, p(t), q(t)) | \psi_j \rangle a_j \tag{2.5}$$

The bosonic bath consists of an M-dimensional coherent state which is produced by a product of M 1-dimensional CS representing a complex number where the phase space coordinates p,q are used in combination to find both the real and imaginary parts.

$$|z_k(t)\rangle = \Pi_{k=1,M} |z^{(k)}(t)\rangle \tag{2.6}$$

Each individual CS represents a complex number

$$z_k(t) = \frac{(\gamma^{\frac{1}{2}} q + i\gamma^{\frac{-1}{2}})}{\sqrt{2}} \tag{2.7}$$

2.1.1 MCEv1

MCEv1 has the ansatz as presented in reference 28,

$$|\Psi(t)\rangle = \sum_{k=1,N} (a_k^{(1)}|1\rangle + a_k^{(2)}|2\rangle)|z_k(t)\rangle \tag{2.8}$$

where a_k are the quantum amplitudes introduced in equation [[[]]], $z_k(t)$ are the CS for each basis function and $|1\rangle$ and $|2\rangle$ represent the different PES in the system, in this case, electronic state 1 and 2. In MCEv1, coupling exists between the different electronic states as well as the different basis functions. The extent of both types of coupling is controlled by the quantum amplitudes.

The equations of motion for the MCE method are derived from the variation principle. This principle states that it is impossible for any approximation of a parameter of the wave function to result in a ground state energy that is a lower than the energy given by the ground state energy calculated by the exact wavefunction. This allows the direct comparison of two parameters of estimation, as the lower ground state energy comes from the better estimator. Calculating the equations requires rewritten the quantum Lagrangian in terms of the quantum amplitudes and the ordered Hamiltonian,

$$\begin{aligned} L = i\left[\frac{a_k^{(1)*}\dot{a}_k^{(1)}}{2} - \frac{a_k^{(1)}\dot{a}_k^{(1)*}}{2}\right] + i\left[\frac{a_k^{(2)*}\dot{a}_k^{(2)}}{2} - \frac{a_k^{(2)}\dot{a}_k^{(2)*}}{2}\right] + \\ i\left[\left(\frac{\dot{z}_k z_k^*}{2} - \frac{z_k \dot{z}_k^*}{2}\right)\left(a_k^{(1)*}a_k^{(1)} + a_k^{(2)*}a_k^{(2)}\right)\right] - H_{11}^{ord}(z_k z_k^*)a_k^{(1)*}a_k^{(1)} \\ -H_{22}^{ord}(z_k z_k^*)a_k^{(2)*}a_k^{(2)} - H_{12}^{ord}(z_k z_k^*)a_k^{(1)*}a_k^{(2)} - H_{21}^{ord}(z_k z_k^*)a_k^{(2)*}a_k^{(1)} \end{aligned} \tag{2.9}$$

Which then after applying the variational principle on the wave function gives,

$$i\dot{z}_k = \frac{\partial H^{Ehr}}{\partial z_k^*} \tag{2.10}$$

while the variational principle on the amplitudes gives the equation,

$$\sum_k i a_k^{(1)} \langle z_j|z_k\rangle - \langle z_j|z_k\rangle \dot{H}^{11}(z_j^*, z_k) a_k^{(1)} - \langle z_j|z_k\rangle \dot{H}^{12}(z_j^*, z_k) a_k^{(2)} + i\left[(z_j^* - z_k^*)\dot{z}_k + \frac{\dot{z_k} z_k^*}{2} - \frac{z_k \dot{z_k^*}}{2}\right] a_k^{(1)} \langle z_j|z_k\rangle \tag{2.11}$$

The end result for the quantum amplitudes can be simplified by rewriting the equation to include classical action and a smooth pre-exponential factor

$$S_k^{(l)} = \int \left[i\frac{\dot{z}_l z_l^* - \dot{z}_l^* z_l}{2} - \langle z|H_u|z\rangle \right] dt \tag{2.12}$$

leading to the equation for the amplitudes,

$$a_k^{(r)} = d_k^{(r)} e^{(iS_k^{(r)})} \tag{2.13}$$

As the wavefunction is comprised of the quantum amplitudes and CS, the MCE method can be propagated from just these equations.

2.1.2 MCEv2

MCEv2 was published with a slightly different ansatz in order to separate the 2 types of coupling, such that the coupling between the PES and the coupling between the individual basis functions are governed by separate variables. In MCEv1 the quantum amplitudes contained total information about coupling such that $a_1^{(1)}$ is coupled to $a_5^{(2)}$. This overburdening of these amplitudes is the motivation of the changes in MCEv2, removing this overlap and therefore allowing for slightly more flexibility with the ansatz,

$$|\Psi(t)\rangle = \sum_{k=1,N} D_k(t)|\psi(t)\rangle = \sum_{k=1,N} D_k(t)(a_k^{(1)}|1\rangle + a_k^{(2)}|2\rangle)|z_k(t)\rangle \tag{2.14}$$

The newly introduced D_k contains the coupling information between the different configurations, leaving the quantum amplitudes $a_k^{(i)}$ to model the coupling in between the PES inside a basis

function. D_k is given by the equation,

$$\sum_{j=1}^{K}\langle\phi_j|\psi_k\rangle\dot{D}_j = -i\sum_{k=1}^{K}\left[\langle\psi_j|\dot{H}|\psi_k\rangle - i\langle\psi_j|\dot{\psi}_k\rangle\right]D_k \tag{2.15}$$

where $\langle\psi_j|\dot{H}|\psi_k\rangle$ is the matrix with elements,

$$\langle\psi_j|\dot{H}|\psi_k\rangle = \sum_{r,s=1}^{R} a_{rj}^{*}a_{sk}\left[\delta_{rs}\langle z_j|\dot{T}|z_k\rangle + \delta_{rs}\langle z_j|V_r(q)|z_k\rangle - \langle z_j|d_{rs}(q)\dot{(q)}|z_k\rangle\right] \tag{2.16}$$

The theory surrounding the CS for both versions of the method is identical and therefore the equations found in the theory of MCEv1 suffice. However the additional flexibility afforded by the new amplitude requires the introduction of a restraint on the basis function, they now need to be normalised (but not orthogonal) for propagation to proceed correctly. This can be ensured by placing the restriction on the quantum amplitudes such that $a^{(1)*}a^{(1)} + a^{(2)*}a^{(2)} = 1$, as the norm of the basis functions is calculated as $\langle\psi|\psi\rangle = a^{(1)*}a^{(1)} + a^{(2)*}a^{(2)} = 1$.

2.2 Cloning

The Ehrenfest trajectories are a vital part of the MCE method and are key for producing useful results while greatly reducing computational time. It is possible, however, given sufficient time, the Ehrenfest trajectories will fail to capture the entire quantum picture and therefore can no longer provide an actionable representation of the system. In order to prevent this loss of information, the computational trick of cloning can be applied, where extra basis functions are generated based on the state of current propagation. This idea has similarities and takes inspiration from the spawning method applied in Ab Inito Multiple Spawning (AIMS).

2.2.1 Cloning in AIMC

AIMC applies cloning to create an additional basis function inside the basis set, whenever the specific basis set struggles to describe the area of phase space required.

$$|\psi_n'\rangle = |\chi_n\rangle\left(\frac{a_I^n}{|a_I^n|}|\psi_I\rangle + \sum_{J\neq I} 0|\psi_J\rangle\right) \tag{2.17}$$

$$|\psi_n''\rangle = |\chi_n\rangle\left(0|\psi_I\rangle + \sum_{J\neq I}\frac{1}{\sqrt{1-|a_I^n|^2}}a_j^n|\psi_J\rangle\right) \tag{2.18}$$

This is required when the 2 PES inside the basis function has excess Ehrenfest force that is unable to handled by propagation and therefore the basis functions ends up 'stuck' and 'straddled', usually occurring after a region of a conical intersection or avoiding crossing. This Ehrenfest force is quantifiable at every timestep and so can be calculated and then compared against the average in order to find excesses,

$$\Delta F_{I,n} = \nabla_R V_I - \sum_J (a_J^n) \nabla_R V_J \tag{2.19}$$

However, as quantum systems are very varied and complex, it is possible that a given state of the system has a negligible impact on the overall wavefunction for a given timestep and there it is sensible to apply a weighting to the calculation of Ehrenfest force for each individual state in order to reduce noise from unnecessary states, and further save computational time,

$$F_{I,n}^{br} = (a_I^n)^* a_I^n \Delta F_{I,n} \tag{2.20}$$

By scaling each force calculation by their quantum amplitudes, the states with negligible population are automatically discarded and the states with the highest populations are favored. The threshold that deems the associated Ehrenfest force excessive and therefore enacts the cloning can be varied in order to better suit the quantum system that is being simulated. When AIMC simulates the spin boson model, it is common practice to simulate only 2 PES, and this has the helpful effect of the potential always having a constant potential. This in turn allows the maximum difference between a states Ehrenfest energy and the average to be found when there is an equivalence between the populations of the 2 states such that, $|a_k^{(1)} a_k^{(2)}|^2 = 0.25$ and so the general threshold is set to $|a_k^{(1)} a_k^{(2)}|^2 > 0.25$. When a basis function exceeds this limit, it is cloned and two new basis functions $|\psi_n'\rangle$ and $|\psi_n'\rangle$ are created,

$$|\psi_n'\rangle = |\chi_n\rangle \left(\frac{a_I^n}{|a_I^n|} |\psi_I\rangle + \sum_{J \neq I} 0 |\psi_J\rangle \right) \tag{2.21}$$

$$|\psi_n''\rangle = |\chi_n\rangle \left(0|\psi_I\rangle + \sum_{J \neq I} \frac{1}{\sqrt{1 - |a_I^n|^2}} a_j^n |\psi_J\rangle \right) \tag{2.22}$$

The clones are calculated in order to retrieve the original basis function after recombination by

simple addition. This is achieved by setting the quantum amplitudes such that their sum is 1 and the contribution to the ith PES is contained within the within the ith clone, which while AIMC is constrained to 2 PES concerns the 2 clones created. At the time of cloning, these clones recombine to exactly form the previous basis function, meaning cloning can be applied without affecting the overall wavefunction, while after propagation they will recombine to essentially give a perturbation of the original basis function, presenting an altered final result.

As time propagation continues, the clones will have contributions from each PES and therefore, given sufficient time, will be indistinguishable from regular basis functions generated at the beginning of propagation, and therefore are subject to the same issues as regular basis functions guided by Ehrenfest trajectories and therefore may require the application of the cloning procedure once again. In order to avoid an endless cascade of clones being created, it is important for the system to propagate before reapplying the cloning procedure. The waiting period is variable and can be altered in order to better represent the system. It is also wise to limit the number of cloning events that can occur over the entire propagation in order to curb the increase in computational cost.

2.3 Spin-Boson model

The Spin-Boson model is one of the most famous models for studying open quantum systems, ones with coupled with an environment and don't exist in isolation. The Spin-Boson model is useful in studying so called two level systems, which is the current area of interest of the MCE method, where a given degree of freedom within the system is restricted to only take one of two values. There exists multiple forms of the spin boson and this report, like previous MCE papers, is going to focus on the model where the spin value is identical in both states at 1/2. This version of the spin boson has a Hamiltonian written as,

$$\hat{H} = \begin{bmatrix} H_B + H_C + \epsilon & \Delta \\ \Delta & H_B - H_C - \epsilon \end{bmatrix} \tag{2.23}$$

Δ, the tunnelling parameter is often given to be 1 and used as a scaling factor. The difference in the zero point energy of the wells is given by ϵ and is called the detuning parameter. The two

Hamiltonians in the equation, H_B and H_C, represent the bosonic bath and the system to bath coupling respectively. Both of these Hamiltonians are able to be rewritten in a way containing only creation and annihilation operators.

$$H_B = \sum_m \omega^{(m)}(\hat{\alpha}^\dagger \hat{\alpha} + \frac{1}{2}) \tag{2.24}$$

$$H_C = \sum_m \frac{C^{(m)}}{\sqrt{2\omega^{(m)}}}(\hat{\alpha}^\dagger + \hat{\alpha}) \tag{2.25}$$

The bosonic bath represented by the Hamiltonian H_B contains information about the M vibrational modes. Each of these modes are important in simulating the continuous vibrational modes present in the physical system and therefore a bath coupled to a particularly complex system will require a large number of bath modes to correct discretise the vibrational modes. Each of the M bath modes are CS which form the bath are as such,

$$|Z_{bath}\rangle = |Z_{(1)}\rangle |Z_{(2)}\rangle \cdot |Z(_M)\rangle) \tag{2.26}$$

The necessary information about the bath modes can be efficiently captured by the spectral density, which denotes all allowed frequencies and the extent of the dampening across the bath. The spectral density and frequency are related via a power law, and the value of that power can be tweaked in order to provide simulations of different systems including multiple solvents or phonons. MCE works primarily with Ohmic spectra,

$$J(\omega) = \frac{\pi}{2} \sum_m \frac{(C^{(m)})^2}{2(\omega^{(m)})^2} \delta(\omega - \omega^{(m)}) \tag{2.27}$$

where the relation between frequency and spectral density is linear up until a specific cut off frequency ω_c after which it is governed by a cut off function, which is chosen to best suit the system. These functions reduce computational time by a large factor as baths tend to exhibit their most important behaviour at lower frequencies. The most common choices of a cut off

function for MCE are the exponential and Drude-Lorentz cut off functions.

$$J_{exp}(\omega) = \frac{\pi}{2}\alpha_k \omega e^{\frac{-\omega}{\omega_c}} \tag{2.28}$$

$$J_{DL}(\omega) = 2\pi\lambda\omega\frac{\Omega}{\Omega^2 + \omega^2} \tag{2.29}$$

The exponential cut off function is a reliable choice as the resulting mathematics is simple due to the introduction of the Kondo parameter representing system to bath coupling. In cases where the number of oscillations has been reduced by the bath, the system is called overdamped and is more suited to a Drude-Lorentz cut off function. The spectral densities produced by these cut off functions are appropriately identical to the point of the cut off where Drude-Lorentz exhibits a longer tail.

Chapter 3

Masters Research to current day

3.1 Cloning in MCEv1 - Masters

Due to the difference in ansatz used in MCEv1 and MCEv2, the cloning procedure has to be implemented in a different way. The MCEv1 ansatz lacks the quantum amplitude D_k separating the forms of coupling, causing the CS to 'push' against each other when in close proximity in phase space. While this is useful for propagation, when clones are created in the same manner as in AIMC, the clones temporarily occupy the same position in phase space creating a singular matrix and causing issues in propagation.

The first potential solution investigated was to shift both clones created in equal but opposite directions in order to reduce the pushing and allow propagation to continue. As the information position and momentum of the CS is contained within its representative complex numbers it suffices to generate a small complex number β and add/subtract that from the generated clones,

$$z'_k = z_k + \beta \tag{3.1}$$

$$z''_k = z_k - \beta \tag{3.2}$$

However, if the size of this shift is too large, the phase space represented by the clones undergoes

too severe of a change that propagation is affected and the trajectories can take an incorrect course, and lead to a recombination that doesn't recover the original nuclear wavefunction. If the shift is too small, the clones push too strongly against each other and creates problems with computation due to singular overlap matrices. After implementing this idea, it was discovered that there is no suitable range that exists and is capable of being generalised beyond given specific systems.

A more costly approach to cloning is not to clone individual straddled basis functions as in AIMC-MCE but to clone the entire basis set. The large increase in cost evidently comes from the substantial increase in basis functions as the number will double at every cloning event. The clones are created as follows,

$$\begin{aligned} |\Psi(t)\rangle = \sum_{k=1,N} (a_k^{(1)}|1\rangle + a_k^{(2)}|2\rangle|z_k(t)\rangle = \sum_{k=1,N} (a_k^{(1)}|1\rangle + 0|2\rangle|z_k(t)\rangle \\ + \sum_{k=1,N} (0|1\rangle + a_k^{(2)}|2\rangle|z_k(t)\rangle \end{aligned} \tag{3.3}$$

As MCEv1 is not beholden to the same normalisation criteria for its basis functions as MCEv2, the clones can be propagated without renormalising and will maintain their norm of 1 when recombined after the final timestep. This creation of an additional basis could be seen as adding an extra repeat to the run starting at specific point as opposed to MCEv2 simply inserting an extra basis function inside the basis set to afford more flexibility. As this approach is relatively computationally expensive, the cloning procedure is set to be applied at given intervals before propagation begins. After the final timestep the clones are recombined in reversed order of creation, to produce 1 complete repetition of the method.

The disadvantage of this version of cloning is that multiple cloning events reintroduces exponential scaling to the basis function therefore creating a exponential scaling in computational time. The choice for the number of cloning events therefore needs to be balanced between accuracy and cost.

The cloning procedure was implemented using these equations such that the clones are created every pre-chosen number of timesteps, and then recombined after every single clone and repetition had been propagated to completion. Cloning in MCEv1 was then tested on a simple spin

boson case that MCEV1 already simulates in great agreement with the benchmark,

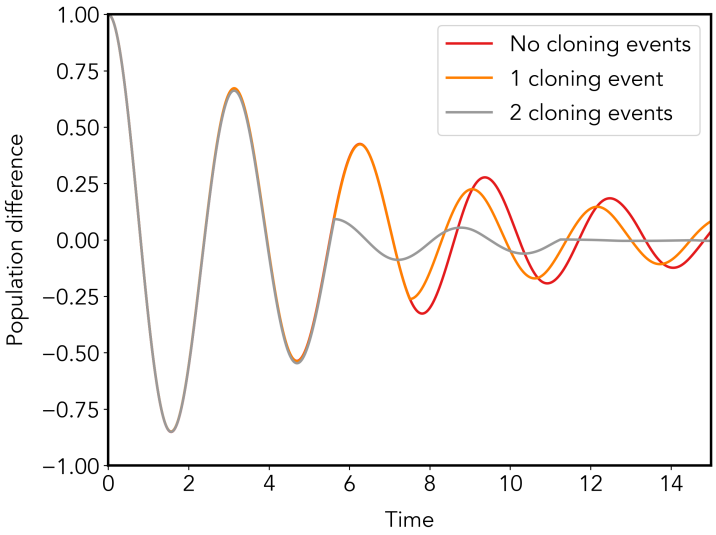

Figure 3.1: First numerical test for cloning in MCEv1. System simulated was the population difference of a Spin-Boson model with symmetrical wells, with parameters $\omega_c/\delta = 2.5$, $\alpha_k = 0.09$, ϵ=0, $\beta\delta$=5. All runs consisted on $N_{rpts} = 32$ repeats and $M = 50$ bath modes and $N_{bfs} = 50$. The cloning procedure was varied for different runs, at time step 1000 (orange) or every 750 timesteps (red).

For this case, and all subsequent tests, the cloning technique caused the propagation of the wavefunction to veer off course. The extent to which this happened depended on the point of cloning. When the symmetrical wells case was cloned with a population difference of approximately 0, the oscillations were incredibly muted. This is because symmetrical wells are invariant to the starting PES as the cost to transfer from one well to the other is identical, resulting in equal but opposite contributions from each clone, essentially cancelling each other out. When the cloning procedure was applied at a point with less even populations, it became clear that cloning in MCEv1 destroys too much information regarding the coupling as the cloned basis sets do not interact, ruining the propagation. When tested upon other systems, similar failings occurred.

3.2 Current PhD research

At the end of my masters research, my supervisor introduced an idea of cloning cross-terms. In the previous working equations, the clones are created to be orthogonal and were assumed to not interact with each other while propagating. However in practice, this assumption requires an infinitely large basis set, and due to the ansatz of MCEv1 containing all of the information about

coupling within the same quantum amplitudes that dictate population of states, interaction between generated clones is required to maintain correct propagation. The populations of each state is then recovered after the final timestep as follows,

$$P_{1,tot} = P_1^{'} + P_1^{''} + P_1^{'-''} + P_1^{''-'} \tag{3.4}$$

$$P_{2,tot} = P_2^{'} + P_2^{''} + P_2^{'-''} + P_2^{''-'} \tag{3.5}$$

where $P_i^{'}$ is the population of the ith state from the first clone and similarly and $P_i^{''}$ is the population of the ith state from the second clone. The newly introduced $P_i^{'-''} + P_i^{''-'}$ are the populations generated by the interactions from clone 1 to clone 2 and the interactions from clone 2 to clone 1 respectively. The populations inside the clone are calculated using the same equations as MCEv1,

$$P_i^{'} = \sum_k \sum_j a_{ik}^{'*} a_{ij}^{'} \langle z_k^{'} | z_j^{'} \rangle \tag{3.6}$$

and the cross terms are calculated in a similar fashion,

$$P_i^{'-''} = \sum_k \sum_j a_{ik}^{'*} a_{ij}^{''} \langle z_k^{'} | z_j^{''} \rangle \tag{3.7}$$

$$P_i^{''-'} = \sum_k \sum_j a_{ik}^{''*} a_{ij}^{'} \langle z_k^{''} | z_j^{'} \rangle \tag{3.8}$$

MCEv1 functions under the condition that the sum of the populations of the PES is normalised such that

$$P_{1,tot} + P_{2,tot} = 1 \tag{3.9}$$

which is carried through the cloning procedure meaning that the new found total probabilities have to be renormalised after final calculations. It is also important to note that the cross terms at time of cloning are exactly zero in order to preserve the proper propagation step. A change in notation to denote the cloning step is also worthwhile, to avoid complication and to allow discussion of multiple cloning events and so the timestep of cloning can be written,

$$\frac{P_1 + P_2}{P_1 + P_2} = \frac{P_1^1 + P_2^1 + P_1^2 + P_2^2 + CT^{\langle 1|2\rangle}}{P_1^1 + P_2^1 + P_1^2 + P_2^2 + CT^{\langle 1|2\rangle}} \tag{3.10}$$

where for the populations the subscript determines the PES and the superscript determines the clone the population refers to. For the cross terms, the absence of a subscript implies that the summation is over all PES while a subscript given denotes a specific PES and the superscript denotes the interactions between which clones. Inside the superscript, a line separator is used to include both permutations of the sum and a comma separator is used for a single permutation, such that

$$CT^{\langle 1|2\rangle} = CT_1^{\langle 1|2\rangle} + CT_2^{\langle 1|2\rangle} \tag{3.11}$$

$$CT_1^{\langle 1|2\rangle} = CT_1^{\langle 1,2\rangle} + CT_1^{\langle 2,1\rangle} \tag{3.12}$$

$$CT_1^{\langle 1,2\rangle} = \sum_k \sum_j a_{1k}^{1*} a_{1j}^2 \langle z_k^1 | z_j^2 \rangle \tag{3.13}$$

$$CT_1^{\langle 2,1\rangle} = \sum_k \sum_j a_{1k}^{2*} a_{1j}^1 \langle z_k^2 | z_j^1 \rangle \tag{3.14}$$

In a second cloning event, all basis sets are cloned, including the clones created in the first event. This causes a further split of the basis functions and the cross terms need to adapt and expand again at the timestep of the second cloning event. Therefore at this timestep,

$$\frac{P_1^1 + P_2^1 + P_1^2 + P_2^2 + CT^{\langle 1|2|3|4\rangle}}{P_1^1 + P_2^1 + P_1^2 + P_2^2 + CT^{\langle 1|2|3|4\rangle}} = \frac{P_1^1 + P_2^1 + P_1^2 + P_2^2 + P_1^3 + P_2^3 + P_1^4 + P_2^4 + CT^{\langle 1|2|3|4\rangle}}{P_1^1 + P_2^1 + P_1^2 + P_2^2 + P_1^3 + P_2^3 + P_1^4 + P_2^4 + CT^{\langle 1|2|3|4\rangle}} \tag{3.15}$$

where the extended cross terms are,

$$CT^{\langle 1|2|3|4\rangle} = CT_1^{\langle 1|2|3|4\rangle} + CT_2^{\langle 1|2|3|4\rangle} \tag{3.16}$$

$$CT_1^{\langle 1|2|3|4\rangle} = CT_1^{\langle 1|2\rangle} + CT_1^{\langle 1|3\rangle} + CT_1^{\langle 1|4\rangle} + CT_1^{\langle 2|3\rangle} + CT_1^{\langle 2|4\rangle} + CT_1^{\langle 3|4\rangle} \tag{3.17}$$

$$CT_2^{\langle 1|2|3|4\rangle} = CT_2^{\langle 1|2\rangle} + CT_2^{\langle 1|3\rangle} + CT_2^{\langle 1|4\rangle} + CT_2^{\langle 2|3\rangle} + CT_2^{\langle 2|4\rangle} + CT_2^{\langle 3|4\rangle} \tag{3.18}$$

As MCEv1 with cloning is propagated using the same equations for regular MCE, the cross terms do not interfere with the propagation and therefore can be calculated entirely after the final timestep in the recombination phase. The true total population of each state is then recovered through the following equations, which have been presented in their form after 1 cloning event for simplicity,

$$P_{1,tot} = P_1^1 + P_1^2 + CT_1^{\langle 1|2\rangle} \tag{3.19}$$

$$P_{2,tot} = P_2^1 + P_2^2 + CT_2^{\langle 1|2\rangle} \tag{3.20}$$

After implementing cross terms into the cloning procedure, MCEv1 was once again tested against the symmetrical well spin-boson model used to test the original cloning procedure.

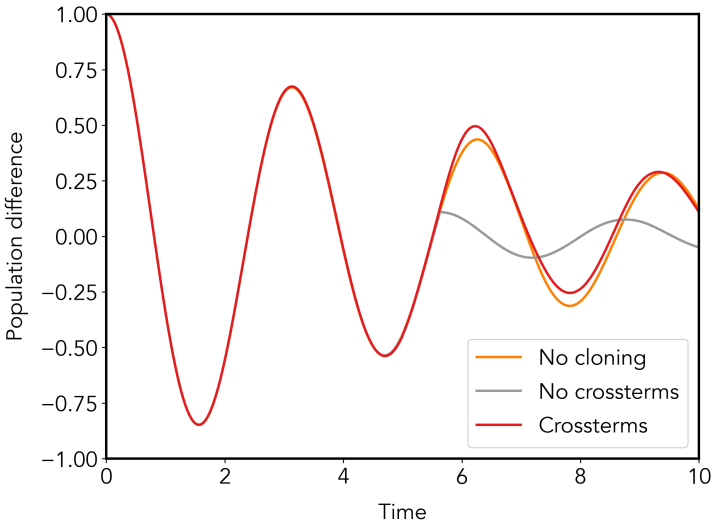

Figure 3.2: First numerical test for cross term cloning in MCEv1. System simulated was the population difference of a Spin-Boson model with symmetrical wells, with parameters $\omega_c/\delta = 2.5$, $\alpha_k = 0.09$, ϵ=0, $\beta\delta$=5. All runs consisted on $N_{rpts} = 32$ repeats and $M = 50$ bath modes and $N_{bfs} = 50$. The orange line is the benchmark as given by MCTDH, the grey line is the original version of cloning in MCEv1 and the red line is given by cloning with cross terms).

The introduction of cross terms has recovered the oscillation behaviour of the system and the oscillations occur perfectly in time with the benchmark, with only the strength of the oscillations being overestimated. This is a great improvement over the derailment of propagation caused by the lack of cross terms, but still requires further research into fully converging the result to MCTDH.

3.3 Future ideas for research

It is possible that a more effective way of preserving the coupling information is instead to rotate the amplitudes instead of setting them to the fixed value. This can be achieved by generating a random number, θ between 1-90 and rotating the quantum amplitudes via trigonometric functions, shown on 1 basis function for simplicity,

$$(a_1|1\rangle + a_2|2\rangle)|z\rangle = (cos^2(\theta)a_1|1\rangle + sin^2(\theta)a_2|2\rangle) + (sin^2(\theta)a_1|1\rangle + cos^2(\theta)a_2|2\rangle) \tag{3.21}$$

this maintains the total wavefunction after additive recombination as summing the two clones produces the original basis function.

$$\begin{aligned} &(cos^2(\theta)a_1|1\rangle + sin^2(\theta)a_2|2\rangle) + (sin^2(\theta)a_1|1\rangle + cos^2(\theta)a_2|2\rangle) \\ &\quad = (cos^2(\theta) + sin^2(\theta))a_1|1\rangle + (cos^2(\theta) + sin^2(\theta))a_2|2\rangle \\ &\quad = (a_1|1\rangle + a_2|2\rangle)|z\rangle \end{aligned} \tag{3.22}$$

This recombination technique works through multiple cloning events by iterating the same trigonometric identity. It is possible that the fact that the amplitudes are not set to 0 allows for more coupling information to be preserved and therefore a more accurate representation of the system to be provided, potentially solving the issues with oscillation strength when combined with the cloning cross terms.

Chapter 4

Research plan

4.1 Training

I have signed up for the Virtual Winter School on Computational Chemistry which will assist me in completing my foundational knowledge. I have also been invited to join a workshop at the Univesity College of London by the plasma chemistry company Quantemol where I hope to see in person applications of the molecular dynamics I am working on in hope of enriching my perspective. There are also several ARK workshops provided by the university which I will take in order to optimise my code for uploading, including the most suitable choices of compilers. I am attending a workshop on GPU coding for python which is a area of coding I know very little about but could speed up my computational time dramatically.

I have also attended a coding workshop here at the university which lead to me rewriting significant portions of my code to include more modulisation and has improved the run speed of my code by a significant factor in several key areas. I am also investing more about Ab Initio dynamics as it's an area I didn't focus on during my masters, but is an area I plan to extend to after finishing cloning in MCEv1.

4.2 Plan

MCEv1 Cross terms:

- Investigate other less easily simulated systems to see improvement due to cross terms.
- Explore if there exists some region of the method to be tweaked (number of basis functions,

repetitions, conditional cloning akin to AIMC etc.) in order to achieve the last part of convergence.

- Rewriting the clone equations to contain rotated amplitudes instead of setting opposite amplitudes to 0

Chapter 5

References

1. Ceotto, M., Tantardini, G.F. and Aspuru-Guzik, A. Fighting the curse of dimensionality in first-principles semiclassical calculations: Non-local reference states for large number of dimensions. Journal of Chemical Physics. 2011, 135(21).

2. Shalashilin, D.V. Multiconfigurational Ehrenfest approach to quantum coherent dynamics in large molecular systems. Faraday Discussions. 2011, 153, pp.105-116.

3. Karplus, M. and Sharma, R.D. Exchange reactions with activation energy .i. simple barrier potential for (H,H2). Journal of Chemical Physics. 1965, 43(9), pp.3259-.

4. Schatz, G.C. Perspective on "Exchange reactions with activation energy. I. Simple barrier potential for (H, H 2)". Theoretical Chemistry Accounts: Theory, Computation, and Modeling (Theoretica Chimica Acta). 2000, 103(3-4), pp.270-272.

5. Schinke, R. Perspective on "Semiclassical theory of atom-diatom collisions: path integrals and the classical S matrix". Theoretical Chemistry Accounts: Theory, Computation, and Modeling (Theoretica Chimica Acta). 2000, 103(3-4), pp.297-299.

6. Miller, W.H. Quantum mechanical transition state theory and a new semiclassical model for reaction rate constants. The Journal of Chemical Physics. 1974, 61(5), pp.1823-1834.

7. Thoss, M. and Wang, H.B. Semiclassical description of molecular dynamics based on initial-value representation methods. Annual Review of Physical Chemistry. 2004, 55, pp.299-332.

8. Miller, W.H. Classical S-Matrix - Numerical Application To Inelastic Collisions. Journal of Chemical Physics. 1970, 53(9), pp.3578-.

9. Miller, W.H. The classical S-matrix: A more detailed study of classically forbidden transitions in inelastic collisions. Chemical Physics Letters. 1970, 7(4), pp.431-435.

10. Miller, W.H. Semiclassical Theory of Atom–Diatom Collisions:Path Integrals and the Classical S Matrix. The Journal of Chemical Physics. 1970, 53 (5), pp.1949-1959.

11. Tannor, D.J. and Garashchuk, S. Semiclassical calculation of chemical reaction dynamics via wavepacket correlation functions. Annual Review of Physical Chemistry. 2000, 51, pp.553-600.

12. Billing, G.D. On the applicability of the classical trajectory equations in inelastic scattering theory. Journal of Chemical physics. 1975, 30, pp.391-393.

13. Heller, E.J. FROZEN GAUSSIANS - A very simple semi-classical approximation. Journal of Chemical Physics. 1981, 75(6), pp.2923-2931.

14. Heller, E.J. Time-dependent approach to semiclassical dynamics. Journal of Chemical Physics. 1975, 62(4), pp.1544-1555.

15. Heller, E.J. Time-dependent variational approach to semiclassical dynamics. Journal of Chemical Physics. 1976, 64(1), pp.63-73.

16. De Leon, N. and Heller, E.J. Semiclassical quantization and extraction of eigenfunctions using arbitrary trajectories. The Journal of Chemical Physics. 1983, 78(6), pp.4005-4017.

17. Sepulveda, M.A. Comment on the breakdown of vanvlecks propagator and its implications for the energy domain greens-function. Progress of Theoretical Physics Supplement. 1994, (116), pp.277-282.

18. Van Vleck, J.H. The Correspondence Principle in the Statistical Interpretation of Quantum Mechanics. Proceedings of the National Academy of Sciences. 1928, 14(2), pp.178-188.

19. Herman, M.F. Time reversal and unitarity in the frozen Gaussian approximation for semiclassical scattering. The Journal of Chemical Physics. 1986, 85(4), pp.2069-2076. 20. Herman, M.F. Dynamics by semiclassical methods. Annual Review of Physical Chemistry. 1994, 45, pp.83-111.

21. Martin-Fierro, E. and Pollak, E. Semiclassical initial value series solution of the spin boson problem. Journal of Chemical Physics. 2007, 126(16).

22. de Aguiar, M.A.M., Vitiello, S.A. and Grigolo, A. An initial value representation for the

coherent state propagator with complex trajectories. Chemical Physics. 2010, 370(1-3), pp.42-50.

23. Bagchi, B., Ghosh, R. and Khare, A. A pedestrian introduction to coherent and squeezed states. International Journal of Modern Physics A. 2020, 35(19).

24. Nieto, M.M. and Simmons, L.M. Coherent states for general potentials. Physical Review Letters. 1978, 41(4), pp.207-210.

25. Schrodinger, E. The constant crossover of micro- to macro mechanics. Naturwissenschaften. 1926, 14, pp.664-666.

26. Nag, J., Menon, V.J. and Mukherjee, S.N. Ehrenfest theorem and the classical trajectory of quantum motion. American Journal of Physics. 1987, 55(9), pp.802-804.

27. Ben-Nun, M., Quenneville, J. and Martinez, T.J. Ab initio multiple spawning: Photochemistry from first principles quantum molecular dynamics. Journal of Physical Chemistry A. 2000, 104(22), pp.5161-5175.

28. Shalashilin, D.V. Quantum mechanics with the basis set guided by Ehrenfest trajectories: Theory and application to spin-boson model. Journal of Chemical Physics. 2009, 130(24).

29. Alptekin, S. Structural phase transition of BeTe: an ab initio molecular dynamics study. Journal of Molecular Modeling. 2017, 23(9).

30. Andriyevsky, B., Doll, K. and Jacob, T. Ab initio molecular dynamics study of lithium diffusion in tetragonal Li7La3Zr2O12. Materials Chemistry and Physics. 2017, 185, pp.210-217.

31. Apra, E., Bhattarai, A., Baxter, E., Wang, S.Y., Johnson, G.E., Govind, N. and El-Khoury, P.Z. Simplified Ab Initio Molecular Dynamics-Based Raman Spectral Simulations. Applied Spectroscopy. 2020, 74(11), pp.1350-1357.

32. Blumberger, J., Tateyama, Y. and Sprik, M. Ab initio molecular dynamics simulation of redox reactions in solution. Computer Physics Communications. 2005, 169(1-3), pp.256-261.

33. Cassone, G., Sponer, J. and Saija, F. Ab Initio Molecular Dynamics Studies of the Electric-Field-Induced Catalytic Effects on Liquids. Topics in Catalysis. 2022, 65(1-4), pp.40-58.

34. Hohl, D. Ab-INITIO MOLECULAR-DYNAMICS - Applications to the molecular and

solid-state physics of phosphorus. Theoretica Chimica Acta. 1995, 91(3-4), pp.237-248.

35. Lespade, L. Ab initio molecular dynamics of free radical-induced oxidation of ergothioneine. Journal of Molecular Modeling. 2019, 25(11).

36. Wang, C., Dai, Y.B., Gao, H.Y., Ruan, X.M., Wang, J. and Sun, B.D. Ab Initio Molecular Dynamics Study of Fe Adsorption on TiN (001) Surface. Materials Transactions. 2010, 51(11), pp.2005-2008.

37. Yamamoto, J. Ab initio molecular dynamics simulation on H2O + C+ reaction. Journal of Molecular Structure-Theochem. 2010, 957(1-3), pp.55-60.

38. Zhang, H., Zhao, J., Pu, Z., Li, Y., Xu, B.Q. and Yang, B. Ab Initio Molecular Dynamic Simulation Of Zn-Al-Fe Alloys. Journal of Mining and Metallurgy Section B-Metallurgy. 2019, 55(1), pp.79-84.

39. Binning, R.C. and Ishikawa, Y. Some recent applications of ab initio electronic structure methods to metal, semimetal, and molecular clusters. Structural Chemistry. 1995, 6(4-5), pp.229-241.

40. Shalashilin, D.V. and Child, M.S. Time dependent quantum propagation in phase space. Journal of Chemical Physics. 2000, 113(22), pp.10028-10036.

41. Shalashilin, D.V. and Child, M.S. Description of tunneling with the help of coupled frozen Gaussians. Journal of Chemical Physics. 2001, 114(21), pp.9296-9304.

42. Child, M.S. and Shalashilin, D.V. Locally coupled coherent states and Herman-Kluk dynamics. Journal of Chemical Physics. 2003, 118(5), pp.2061-2071.

43. Shalashilin, D.V. and Child, M.S. Nine-dimensional quantum molecular dynamics simulation of intramolecular vibrational energy redistribution in the CHD3 molecule with the help of coupled coherent states. Journal of Chemical Physics. 2003, 119(4), pp.1961-1969.

44. Shalashilin, D. and Child, M. Quantum propagation on trajectory guided random grids of coupled coherent states. Abstracts of Papers of the American Chemical Society. 2004, 227, pp.U279-U279.

45. Shalashilin, D.V. and Child, M.S. Real time quantum propagation on a Monte Carlo trajectory guided grids of coupled coherent states: 26D simulation of pyrazine absorption spectrum.

Journal of Chemical Physics. 2004, 121(8), pp.3563-3568.

46. Shalashilin, D.V., Child, M.S. and Clary, D.C. Quantum initial value representation simulation of water trimer far infrared absorption spectrum. Journal of Chemical Physics. 2004, 120(12), pp.5608-5615.

47. Green, J.A. and Shalashilin, D.V. Simulation of the quantum dynamics of indistinguishable bosons with the method of coupled coherent states. Physical Review A. 2019, 100(1).

48. Green, J.A., Grigolo, A., Ronto, M. and Shalashilin, D.V. A two-layer approach to the coupled coherent states method. Journal of Chemical Physics. 2016, 144(2).

49. Shalashilin, D.V. Nonadiabatic dynamics with the help of multiconfigurational Ehrenfest method: Improved theory and fully quantum 24D simulation of pyrazine. Journal of Chemical Physics. 2010, 132(24).

50. Tanimura, Y. Nonperturbative expansion method for a quantum system coupled to a harmonic-oscillator bath. Physical Review A. 1990, 41(12), pp.6676-6687.

51. Tanimura, Y. and Kubo, R. Time Evolution of a Quantum System in Contact with a Nearly Gaussian-Markoffian Noise Bath. Journal of the Physical Society of Japan. 1989, 58(1), pp.101-114.

52. Tanimura, Y. Reduced hierarchical equations of motion in real and imaginary time: Correlated initial states and thermodynamic quantities. Journal of Chemical Physics. 2014, 141(4).

53. Zheng, X., Xu, R.X., Xu, J., Jin, J.S., Hu, J. and Yan, Y.J. Hierarchical Equations of Motion for Quantum Dissipation and Quantum Transport. Progress in Chemistry. 2012, 24(6), pp.1129-1152.

54. Noack, M., Reinefeld, A., Kramer, T., Steinke, T. and Ieee. DM-HEOM: A Portable and Scalable Solver-Framework for the Hierarchical Equations of Motion. In: 32nd IEEE International Parallel and Distributed Processing Symposium (IPDPS), May 21-25, Vancouver, CANADA. 2018, pp.947-956.

55. Iles-Smith, J., Lambert, N. and Nazir, A. Environmental dynamics, correlations, and the emergence of noncanonical equilibrium states in open quantum systems. Physical Review A. 2014, 90(3).

56. Iles-Smith, J., Dijkstra, A.G., Lambert, N. and Nazir, A. Energy transfer in structured and unstructured environments: Master equations beyond the Born-Markov approximations. The Journal of Chemical Physics. 2016, 144(4), p.044110.

57. Wilhelm, F.K., Kleff, S. and von Delft, J. The spin-boson model with a structured environment: a comparison of approaches. Chemical Physics. 2004, 296(2), pp.345-353.

58. Leggett, A.J., Chakravarty, S., Dorsey, A.T., Fisher, M.P.A., Garg, A. and Zwerger, W. Dynamics of the dissipative two-state system. Reviews of Modern Physics. 1987, 59(1), pp.1-85.

59. Makhov, D.V., Symonds, C., Fernandez-Alberti, S. and Shalashilin, D.V. Ab initio quantum direct dynamics simulations of ultrafast photochemistry with Multiconfigurational Ehrenfest approach. Chemical Physics. 2017, 493, pp.200-218.

60. Makhov, D.V., Glover, W.J., Martinez, T.J. and Shalashilin, D.V. Ab initio multiple cloning algorithm for quantum nonadiabatic molecular dynamics. Journal of Chemical Physics. 2014, 141(5).

61. Freixas, V.M., Fernandez-Alberti, S., Makhov, D.V., Tretiak, S. and Shalashilin, D. An ab initio multiple cloning approach for the simulation of photoinduced dynamics in conjugated molecules. Physical Chemistry Chemical Physics. 2018, 20(26), pp.17762-17772.

62. Megna, M., Lembo, S., Balato, N. and Monfrecola, G. "Active" photoprotection: sunscreens with DNA repair enzymes. Giornale Italiano Di Dermatologia E Venereologia. 2017, 152(3), pp.302-307.

63. Wolf, P. Topical DNA repair enzymes: A novel approach to photoprotection. Journal of Investigative Dermatology. 2006, 126, pp.S19-S19.

64. Rodrigues, N.D.N., Cole-Filipiak, N.C., Blodgett, K.N., Abeysekera, C., Zwier, T.S. and Stavros, V.G. Wavepacket insights into the photoprotection mechanism of the UV filter methyl anthranilate. Nature Communications. 2018, 9.

65. De Vico, L., Page, C.S., Garavelli, M., Bernardi, F., Basosi, R. and Olivucci, M. Reaction Path Analysis of the "Tunable" Photoisomerization Selectivity of Free and Locked Retinal Chromophores. Journal of the American Chemical Society. 2002, 124(15), pp.4124-4134.

66. Ruhman, S., Hou, B.X., Friedman, N., Ottolenghi, M. and Sheves, M. Following evolution of bacteriorhodopsin in its reactive excited state via stimulated emission pumping. Journal of

the American Chemical Society. 2002, 124(30), pp.8854-8858.

67. Hayashi, S., Tajkhorshid, E. and Schulten, K. Molecular Dynamics Simulation of Bacteriorhodopsin's Photoisomerization Using Ab Initio Forces for the Excited Chromophore. Biophysical Journal. 2003, 85(3), pp.1440-1449.

68. Woolf, T.B. Molecular dynamics simulations of individual bacteriorhodopsin helices. Biophysical Journal. 1996, 70(2), pp.WAML8-WAML8.

69. Edholm, O. and Jahnig, F. Molecular-dynamics simulations of bacteriorhodopsin. In: 25th Jerusalem Symp on Quantum Chemistry and Biochemistry, May 18-21, Jerusalem, Israel. 1992, pp.47-60.

70. Watanabe, M., Soosaar, K. and Chun, H.M. Multigranular molecular dynamics simulations of Bacteriorhodopsin. Abstracts of Papers of the American Chemical Society. 1998, 216, pp.U687-U687.

71. Mathies, R.A., Cruz, C.H.B., Pollard, W.T. and Shank, C.V. Direct observation of the femtosecond excited-state cis-trans isomerization in bacteriorhodopsin. Science. 1988, 240(4853), pp.777-779.

72. Hou, B., Friedman, N., Ruhman, S., Sheves, M. and Ottolenghi, M. Ultrafast spectroscopy of the protonated Schiff bases of free and C-13=C-14 locked retinals. Journal of Physical Chemistry B. 2001, 105(29), pp.7042-7048.

73. Makhov, D.V., Saita, K., Martinez, T.J. and Shalashilin, D.V. Ab initio multiple cloning simulations of pyrrole photodissociation: TKER spectra and velocity map imaging. Physical Chemistry Chemical Physics. 2015, 17(5), pp.3316-3325.

74. Green, J.A., Makhov, D.V., Cole-Filipiak, N.C., Symonds, C., Stavros, V.G. and Shalashilin, D.V. Ultrafast photodissociation dynamics of 2-ethylpyrrole: adding insight to experiment with ab initio multiple cloning. Physical Chemistry Chemical Physics. 2019, 21(7), pp.3832-3841.

75. Makhov, D.V., Martinez, T.J. and Shalashilin, D.V. Toward fully quantum modelling of ultrafast photodissociation imaging experiments. Treating tunnelling in the ab initio multiple cloning approach. Faraday Discussions. 2016, 194, pp.81-94.

76. Makhov, D.V., Adeyemi, S., Cowperthwaite, M. and Shalashilin, D.V. Simulation of the dynamics of vibrationally mediated photodissociation for deuterated pyrrole. Journal of Physics

Communications. 2022, 6(2).

77. Symonds, C.C., Makhov, D.V., Cole-Filipiak, N.C., Green, J.A., Stavros, V.G. and Shalashilin, D.V. Ultrafast photodissociation dynamics of pyrazole, imidazole and their deuterated derivatives using ab initio multiple cloning. Physical Chemistry Chemical Physics. 2019, 21(19), pp.9987-9995.

78. Makhov, D.V. and Shalashilin, D.V. Simulation of the effect of vibrational pre-excitation on the dynamics of pyrrole photo-dissociation. Journal of Chemical Physics. 2021, 154(10).